INTERNATIONAL JOURNAL OF AGRICULTURE & BIOLOGY
ISSN Print: 1560–8530; ISSN Online: 1814–9596
17F–078/2017/19–6–1576–1584
DOI: 10.17957/IJAB/15.0475
http://www.fspublishers.org

Full Length Article

Using Combined Vegetation Indices to Monitor Leaf Chlorophyll Content in Winter Wheat Based on Hj-1a/1b Images

Changwei Tan*, Jian Zhou, Ming Luo, Ying Du, Xin Yang and Chang Ma
Jiangsu Key Laboratory of Crop Genetics and Physiology/Co-Innovation Center for Modern Production Technology of Grain Crops, Yang zhou University, Yang zhou 225009, China
*For correspondence: tanwei010@126.com

Abstract

This article investigates the relationships between leaf chlorophyll content (LCC) and these combination variables derived from vegetation indices, which are extracted from HJ-1A/1B images. The combined models – new measures of monitoring LCC, are compared to single vegetation index model. The results demonstrate that normalization combination for normalized difference vegetation index (NDVI) and green normalized difference vegetation index (GNDVI), namely N (NDVI, GNDVI), is feasible to monitor winter wheat LCC at jointing stage (node formation). R^2 and RMSE are 0.861 and 0.345, respectively, which are more ideal than those of single vegetation index model. The accuracy increases by 3.4%. Ratio combination for NDVI and GNDVI, namely R (NDVI, GNDVI), is feasible to monitor LCC at booting stage. R2 and RMSE are 0.616 and 0.208, respectively, which are more ideal than those of single vegetation index model. The accuracy increases by 15.1%. Difference combination for NDVI and GNDVI, namely D (NDVI, GNDVI), is feasible to monitor LCC at anthesis. R2 and RMSE are 0.694 and 0.409, respectively, which are more ideal than those of single vegetation index model. The accuracy increases by 13%. In conclusion, the combined models can provide a new method for accurately monitoring crop growth conditions in the future. © 2017 Friends Science Publishers

Keywords: Winter wheat; HJ-1A/1B images; Remote sensing; Combined vegetation indices; Leaf chlorophyll content; Growth stages; Monitoring models

Introduction

Leaf chlorophyll content (LCC) is an indicator of crop substance transfer and energy change and an important index to evaluate photosynthetic capacity. It could also indirectly reflect the health status of crops, which is an indispensable index in remote sensing agricultural monitoring (Gitelson *et al*., 2012; Feng *et al*., 2015; Tan *et al*., 2015).

Many domestic and foreign scholars have carried out research on LCC prediction based on crop leaf reflectance characteristics (Soummer *et al*., 2007; Guizar-Sicairos *et al*., 2008). The rapid acquisition of LCC is also important for the study of primary productivity of crops. Remote sensing monitoring is dominated by hyper spectral and multi spectral data. In the principle of remote sensing monitoring, the correlation between LCC and reflectance spectrum has been studied in experiments (Horler *et al*., 1983), and some studies have shown that the position and shape of the red edge of the spectrum can be employed as indicators of monitoring the vegetation physic chemical parameters (LCC, etc.) (Curran *et al*., 1990; Filella and Penuelas, 1994). Subsequently, a multivariate statistical method based on the monitoring of LCC was extensively developed (Wessman *et al*., 1988; Yoder and Pettigrew-Crosby, 1995). Clever sand Gitelson (2013) sought a common sensitive band or combination of LCC and leaf nitrogen content based on multispectral data. Amar *et al*. (2016) found that the proposed image processing technique of LCC measurement would be a good alternative for measuring LCC rapidly and with ease. With its good precision and fast processing, the symbolic regression algorithm was a powerful tool for remote sensing of LCC that could be used advantageously in the reprocessing of large data sets (Tan *et al*., 2012). Gitelson *et al*. (2003) proved that reflectance measurement makes it possible to quickly and non-destructively assess, in situ, the LCC in leaves. Simple and robust algorithms were explored for spectral assessment of LCC using the diverse hyper spectral data sets for six vegetation types acquired in four locations (Japan, France, Italy and USA) (Yoshio *et al*., 2016). Kelly and Yuhong (2013) developed and evaluated a species percent cover-based LCC scaling up procedure in order to accurately estimate crop LCC at canopy or landscape level. Adaptive Network-based Fuzzy Inference System (ANFIS) model which was a good method to be applied to hyper spectral data for estimation of vegetation LCC can greatly improve vegetation LCC estimation accuracy (Yao *et al*., 2010). Previous results showed that

To cite this paper: Tan, C., J. Zhou, M. Luo, Y. Du, X. Yang and C. Ma, 2017. Using combined vegetation indices to monitor leaf chlorophyll content in winter wheat based on Hj-1a/1b images. *Int. J. Agric. Biol*., 19: 1576–1584

good estimates of LCC were feasible using ratio vegetation index (RVI) obtained from hyper spectral data (Kooistra and Clevers, 2016). Many researchers have demonstrated the feasibility of using canopy reflectance spectros copy to detect crop LCC (Al-Abbas *et al*., 1974; Hinzman *et al*., 1986).

The majority of the above cited studies presented empirical evidence suggesting a functional relationship between crop LCC and remote sensing vegetation indices, and these were mostly focused on hyper spectral data or single remote sensing vegetation index. There were only few reports on quantitatively monitoring LCC for winter wheat canopy using the combination of remote sensing vegetation indices extracted from satellite images. Besides, the relationships differed from one eco system type to another eco system due to the influences of vegetation type, strong background signals, canopy structure and spatial heterogeneity. Further, existing remote sensing-based LCC products lacked adequate ground validation, which was critical for establishing the uncertainty and accuracy of such products so that they could be used for guiding crop production practices (Tan *et al*., 2015).

The objective of the present study was to develop a method of further optimizing remote sensing monitoring model of winter wheat LCC at key growth stages. Sensitive vegetation indices or their combinations were adopted by the comprehensive analysis of LCC and multi-spectral satellite remote sensing vegetation index at critical growth stage, while taking the differences between HJ-1A/1B multi spectral data (spatial resolution=30 m and time resolution=2 d) and the quantitative relationship between the ratio and the normalized combination under consideration at the same time. It can be employed to establish a comprehensive monitoring model of remote sensing vegetation index combination.

Materials and Methods

Experimental Details

Three field experiments were performed. In all these experiments, the varieties of winter wheat (*Triticum aestivum* L.) used wereYang Mai 158, Yang Mai 16. First field experiment was conducted from March to April in 2012 in Tai Xing City, Jiang Yan District, Xing Hua City, and Da Feng District in Jiangsu Province, P.R. China. A total of 66 sampling sites were set (15–20 in each study area). Second field experiment was conducted from March to May in 2013 in Tai Xing City, Jiang Yan District, Xing Hua City, and Gao You City in Jiangsu Province, P.R. China. A total of 60 sampling sites were set (10–20 in each study area). Third field experiment was conducted from March to April in 2014 in Yi Zheng City, Jiang Yan District, Xing Hua City, Tai Xing City, and Da Feng District in Jiangsu Province, P.R. China. A total of 104 sampling sites were set (15–25 in each study area).

Study Areas

Study areas are in the central region of Jiangsu Province (119°12′-120°26′ E, 32°2′-33°16′ N), which is one of the main winter wheat production areas in Jiangsu. The areas have sub-tropical moist monsoon climate, dish-shaped plain depression, about 1000 mm annual average precipitation, and about 2200 h annual average sunshine. Rice is the fore-rotating crop in study areas.

Field Investigation and Laboratory Tests

The sampling sites in study areas were relatively uniform and scattered. Geographical location information of each sampling site was collected by Juno ST hand held GPS (Trimble Company, United States). Sampling periods have been determined by actual field investigation, including jointing stage, booting stage and anthesis. Field investigation failed to detect any significant difference of winter wheat growth conditions from 2012 to 2014 in the same periods. Representative large fields that had uniform seedling growth and the best uniform management were chosen randomly as sampling points. These sampling points were at least 60 m away from field boundaries. Sampling sites in different winter wheat growth stages were kept as close as those in the first stage. Four rows (50 cm) of winter wheat plants with uniform growth conditions were chosen in the central region of each study area. Meanwhile, GPS positioning was applied, and geographic information was recorded.

A total of 15–20 winter wheats, which sampled with soil, were selected at each sampling point at jointing stage, booting stage and anthesis, respectively. The samples were put into different net bags divided by the sampling points and were labeled with winter wheat variety and location information. Useful leaves, which were the growth and development of normal, pest free and fresh leaves, were selected, preserved in a dark place and promptly sent to the laboratory. The samples were taken out, tested at the place where the light was off, chopped up and then mixed uniformly. We accurately weighed 0.5 g samples in a mortar, added 25 mL acetone with 80%, grinded and then filtered into a 50 mL volumetric flask. After wards, the mortar and filter paper must be washed with 80% acetone, and the lotion was put into the volumetric flask. Furthermore, the volume was fixed to 50 mL. At last, the spectrophotometric method was employed to measure LCC. At last, the spectrophotometric method was employed to measure LCC (Laval-Martin, 1985).

Remote Sensing Images and Processing

Remote sensing images on sampling dates in this paper were 2A HJ-1A/1B images, which were provided free by China Centre for Resources Satellite Data and Application. The research employed 9 HJ-1A/1B images, and acquisition

dates of the satellite images were coincident with winter wheat growth stages, namely, including 20120309, 20130312 and 20140303 at jointing stage, 20120412, 20130414 and 20140410 at booting stage, and 20120428, 20130501 and 20140424 at anthesis, respectively.

HJ-1A/1B images were preprocessed by ENVI5.1 software. First, rough geometric correction of HJ-1A/1B images was conducted by the 1:100,000 topographic map of Jiangsu Province. Next, refined geometric correction of HJ-1A/1B images was performed by GPS control points, which were obtained by ground measurement. Atmospheric correction and reflectivity conversion were accomplished by empirical linear conversion (Tan *et al*., 2015).

Representative water body in the study areas was chosen as the low-reflectivity calibration object and open cement pavement was employed as high-reflectivity calibration object. HJ-1A/1B image scaling was implemented by manual calibration. The radiance formula, which was employed to convert digital number (DN) value images into radiance images based on absolute calibration coefficient, is as follows (Equation (1)):

$$L=DN/a+L_0 \quad (1)$$

Where L is radiance, a is gains of the absolute calibration coefficient and L_0 is off set. The converted radiance unit is $W.m^{-2}.sr^{-1}.\mu m^{-1}$.

Remote Sensing Vegetation Indices

Common remote sensing vegetation indices corresponding to LCC were chosen according to the literature. Spectral reflectance corresponding to sampling sites of GPS positioning was extracted by ENVI 5.1 software. Next, satellite remote sensing vegetation indices of each sampling site were calculated by combining existing algorithms of satellite remote sensing indices (Table 1).

Combinations of different Remote Sensing Vegetation Indices

Eight common remote sensing vegetation indices were chosen, namely, normalized difference vegetation index (NDVI), nitrogen reflectance index (NRI), green normalized difference vegetation index (GNDVI), structure intensive pigment index (SIPI), plant senescence reflectance index (PSRI), difference vegetation index (DVI), ratio vegetation index (RVI) and enhanced vegetation index (EVI). They were combined in pairs by difference calculation, ratio calculation and normalization calculation. Here, A and B were taken for example. Difference combination, ratio combination and normalization combination were defined D (A, B) = A - B, R (A, B) = A/B and N (A, B) = (A - B)/(A + B), respectively. Therefore, a total of $28\times3=84$ combinations were gained to promise diversity and reliability at jointing stage, booting stage and anthesis.

Data Analysis and Utilization

Relationships between different remote sensing vegetation indices and their combinations and LCC at jointing stage, booting stage and anthesis were analyzed by SPSS18.0. The remote sensing monitoring model of regional winter wheat seedling parameters in major growth periods was established by the strongest correlations in exponential, linear, logarithmic, quadratic polynomial (here in after referred to as polynomial) and power correlation models. Subsequently, the 1:1 relation diagram between predicted LCC values and measured LCC values was drawn to evaluate the established model. Data from the field experiments in 2013 (60 samples) and 2014 (104 samples) were together used to develop the remote sensing monitoring models, and data from the field experiments in 2012 (66 samples) were used to evaluate the models. Accuracy of the remote sensing monitoring model was assessed by the coefficient of determination (R^2) and root mean square error (RMSE). RMSE was computed according to Equation (2). Moreover, the spatial quantization diagram of LCC grade distribution at different stages in the central region of Jiangsu Province was drawn with ArcGIS 10.3 software.

$$RMSE=\sqrt{\frac{1}{n}\sum_{i=1}^{n}(y_i-\hat{y}_i)^2} \quad (2)$$

Where, y_i and $\hat{y}_i$ indicate measured values and predicted values, respectively; n represent number of samples.

Results

Distribution of LCC

In this paper, we used the 2013 and 2014 data as training set to develop the remote sensing monitoring models, and used 2012 data as test set to evaluate the models. Table 2 showed that the amplitude, average, standard deviation and standard error of samples of training set and test set were similar. And the training set and the test set are independent of each other. Thus, it is reliable to establish and validate the model using these data sets.

Relationships between Remote Sensing Vegetation Indices, their Combinations and Winter Wheat LCC at different Growth Stages

Viewed from individual jointing (node formation), booting and anthesis stages, it was easy to find by comparing Tables 3 and 4 that most of the combinations were most strongly correlated to LCC ($P < 0.01$). Furthermore, according to comparisons of r, at jointing stage, the normalization combination of NDVI and GNDVI,

Table 1: Common satellite remote sensing vegetation indices

Vegetation index	Calculating formula
Normalized difference vegetation index (NDVI)	NDVI=(B4-B3)/(B4+B3)
Nitrogen reflectance index (NRI)	NRI=(B2-B3)/(B2+B3)
Green normalized difference vegetation index (GNDVI)	GNDVI=(B4-B2)/(B4+B2)
Structure intensive pigment index (SIPI)	SIPI=(B4-B1)/(B4+B1)
Plant senescence reflectance index (PSRI)	PSRI=(B3-B1)/ B4
Difference vegetation index (DVI)	DVI= B4-B3
Ratio vegetation index (RVI)	RVI= B4/B3
Enhanced vegetation index (EVI)	EVI= 2.5*(B4-B3) /(B4+6*B3-7.5*B2+1)

Note: B1, B2, B3 and B4 denoted spectrum reflectance at blue, green, red and near infrared bands, respectively. The same as below

Table 2: Distribution of LCC in training and test datasets

Year	Sample size	Period	Maximum value	Minimum value	Average value	Standard deviation	Standard error
2012	66	Jointing stage	5.514	3.778	4.688	1.748	0.215
		Booting stage	5.519	4.448	5.149	0.372	0.046
		Anthesis	6.288	4.517	5.408	0.887	0.109
2013	60	Jointing stage	5.467	3.488	4.716	1.603	0.207
		Booting stage	5.522	4.498	5.233	0.308	0.041
		Anthesis	6.072	4.46	5.371	0.809	0.104
2014	104	Jointing stage	5.762	3.963	5.08	1.463	0.143
		Booting stage	5.813	4.782	5.553	0.441	0.043
		Anthesis	6.302	4.847	5.671	0.727	0.071

Table 3: Correlation coefficients between vegetation indices and winter wheat LCC in the key period

Vegetation Index	NDVI	NRI	GNDVI	SIPI	PSRI	DVI	RVI	EVI
Jointing stage	0.604**	0.480**	-0.677**	-0.329**	-0.390**	0.402**	0.414**	0.354**
Booting stage	0.452**	0.348**	-0.612**	-0.281**	-0.402**	0.284**	0.204**	0.258**
Anthesis	0.567**	0.399**	-0.674**	-0.429**	-0.143**	-0.447**	-0.382**	-0.518**

Note:*: P <0.05; **: P <0.01.The same as below

namely N (NDVI, GNDVI), had the highest correlation coefficient in all three types of combinations, which was higher than that of single vegetation index. Comprehensively, N (NDVI, GNDVI) had a stronger correlation ($r = 0.838$, $P < 0.01$) than R (NDVI, GNDVI) and D (NDVI, GNDVI). Therefore, LCC inversion by N (NDVI, GNDVI) was feasible at jointing stage according to the principle of sensitive parameter determination. At booting stage, the ratio combination of NDVI and GNDVI, namely R (NDVI, GNDVI), had the highest correlation coefficient in all three types of combinations, which was higher than that of single vegetation index. Comprehensively, R (NDVI, GNDVI) had stronger correlation ($r = 0.819$, $P < 0.01$) than D (NDVI, GNDVI) and N (NDVI, GNDVI). Therefore, LCC inversion by R (NDVI，GNDVI) was feasible at booting stage according to the principle of sensitive parameter determination. At anthesis, the difference combination of NDVI and GNDVI, namely D (NDVI, GNDVI), had the highest correlation coefficient in all three types of combinations, which was higher than that of single vegetation index. Comprehensively, D (NDVI, GNDVI) had stronger correlation ($r = 0.803$, $P < 0.01$) than R (NDVI, DVI) and N (NDVI, GNDVI). Therefore, LCC inversion by D (NDVI, GNDVI) was feasible at anthesis according to the principle of sensitive parameter determination.

Establishment of Remote Sensing Vegetation Indices Combined Model of Winter Wheat LCC at different Growth Stages

Based on the principle of the strongest correlation and above analysis results, N (NDVI, GNDVI), R (NDVI, GNDVI) and D (NDVI, GNDVI) were chosen to monitor winter wheat LCC at jointing stage, booting stage and anthesis, respectively. Next, the sensitive combinations were employed as independent variables and LCC was employed as the dependent variable to establish remote sensing monitoring models of winter wheat LCC at jointing stage, booting stage and anthesis by exponential, linear, logarithmic, polynomial and power modeling methods (Table 5).

Formulas with the highest R^2 were determined as the remote sensing monitoring models of winter wheat LCC at jointing stage, booting stage and anthesis (Fig. 1). Specifically, among them, LCC had the closet linear relation with the combination of N (NDVI, GNDVI) at jointing stage. The monitoring model of winter wheat LCC at jointing stage was established by linear method ($R^2 = 0.702$, $P < 0.01$). At booting stage, LCC had the closet polynomial relation with the combination of R (NDVI, GNDVI). The monitoring models of winter wheat LCC at booting stage was established by polynomial method ($R^2 = 0.684$).

Table 4: Correlation coefficients between combinations of vegetation indices and winter wheat LCC in the key periods (Jointing stage, Booting stage, Anthesis)

Vegetation index combination	Difference combination	Ratio combination	Normalized combination
(NDVI，NRI)	(0.362**，0.319**，0.582**)	(-0.430**，-0.315**，-0.081)	(-0.516**，-0.068，-0.074)
(NDVI，GNDVI)	(0.725**，0.752**，0.803**)	(0.805**，0.819**，0.692**)	(0.838**，0.797**，0.751**)
(NDVI，SIPI)	(0.658**，0.642**，0.729*)	(0.693**，0.679**，0.640**)	(0.700**，0.671**，0.675**)
(NDVI，PSRI)	(0.637**，0.653**，0.641**)	(0.612**，0.602**，0.160)	(0.645**，0.622**，0.488**)
(NDVI，DVI)	(-0.402**，-0.345**，0.406**)	(0.295**，0.222**，0.746**)	(0.329**，0.223**，0.682**)
(NDVI，RVI)	(-0.367**，-0.239**，0.479**)	(0.151*，0.272**，0.639**)	(0.141*，0.266**，0.630**)
(NDVI，EVI)	(-0.291**，-0.276**，0.567**)	(-0.080，0.032，0.496**)	(-0.089，-0.032，0.572**)
(NRI，GNDVI)	(0.690**，0.601**，0.742**)	(0.249**，0.181**，0.590**)	(0.226**，0.086，0.613**)
(NRI，SIPI)	(0.534**，0.369**，0.517*)	(0.382**，0.303**，0.496**)	(0.387**，0.214**，0.511**)
(NRI，PSRI)	(0.534**，0.476**，0.518**)	(0.260**，0.147*，0.160*)	(0.008，-0.034，-0.046)
(NRI，DVI)	(-0.402**，-0.345**，0.406**)	(0.530**，0.449**，0.572**)	(0.542**，0.404**，0.550**)
(NRI，RVI)	(-0.385**，-0.270**，0.385**)	(0.518**，0.410**，0.497**)	(0.529**，0.366**，0.501**)
(NRI，EVI)	(-0.327**，-0.313**，0.505**)	(0.366**，0.241**，0.476**)	(0.283**，0.096，0.505**)
(GNDVI，SIPI)	(-0.225，-0.236**，-0.518**)	(-0.365**，-0.387**，-0.494**)	(-0.441**，-0.372**，-0.509**)
(GNDVI，PSRI)	(-0.364**，-0.271**，-0.653**)	(-0.024，0.025，0.089)	(-0.051，0.036，0.322**)
(GNDVI，DVI)	(-0.402**，-0.345**，0.406)	(-0.644**，-0.578**，-0.086)	(-0.636**，-0.553**，-0.129)
(GNDVI，RVI)	(-0.455**，-0.359**，0.247**)	(-0.625**，-0.545**，-0.240**)	(-0.656**，-0.543**，-0.262**)
(GNDVI，EVI)	(-0.402**，-0.380**，0.351**)	(-0.415**，-0.294**，0.122)	(-0.478**，-0.382**，0.146*)
(SIPI，PSRI)	(-0.082，0.031，-0.339**)	(0.206**，0.264**，0.107)	(0.237**，0.275**，0.351**)
(SIPI，DVI)	(-0.402**，-0.345**，0.406**)	(-0.481**，-0.401**，0.290**)	(-0.450**，-0.385**，0.244**)
(SIPI，RVI)	(-0.439**，-0.342**，0.321**)	(-0.497**，-0.388**，0.137*)	(-0.397**，-0.388**，0.117)
(SIPI，EVI)	(-0.385**，-0.357**，0.431**)	(-0.356**，-0.226**，0.283**)	(-0.397**，-0.300**，0.333**)
(PSRI，DVI)	(-0.403**，-0.345**，0.406**)	(-0.473**，-0.468**，-0.288**)	(-0.468**，-0.464**，-0.330**)
(PSRI，RVI)	(-0.428**，-0.330**，0.360**)	(-0.479**，-0.442**，-0.316**)	(-0.496**，-0.445**，-0.348**)
(PSRI，EVI)	(-0.370**，-0.354**，0.483**)	(-0.364**，-0.287**，-0.174**)	(-0.391**，-0.347**，-0.211**)
(DVI，RVI)	(0.402**，0.354**，-0.406**)	(-0.115，0.009，-0.133*)	(-0.193**，-0.010，-0.177*)
(DVI，EVI)	(0.402**，0.354**，-0.406**)	(-0.189**，-0.079，0.179*)	(-0.224**，-0.131*，0.213**)
(RVI，EVI)	(0.123，-0.087，0.068)	(-0.204**，-0.149*，0.223**)	(-0.154*，-0.173*，0.296**)

Note:The three values from left to right in parentheses show the correlation coefficients at jointing stage, booting stage and anthesis, respectively.Bold figures mean the best significance

Table 5: Model of winter wheat LCC based on remote sensing vegetation indicescombinations through different modeling method

Period	modeling method	Formula	R^2
Jointing stage	Exponential function	$y = 4.6573e^{0.5534x}$	0.701
	Linear function	$y = 2.5613x + 4.6775$	0.702
	Logarithmic function	No result.	
	Polynomial function	$y = 0.1008x^2 + 2.5639x + 4.6754$	0.701
	power function	No result.	
Booting stage	Exponential function	$y = 3.4635e^{0.3441x}$	0.661
	Linear function	$y = 1.643x + 3.2638$	0.670
	Logarithmic function	$y = 1.4871\ln(x) + 4.9456$	0.675
	Polynomial function	$y = -0.48458x^2 + 2.5716x + 2.8449$	0.684
	Power function	$y = 4.9273x^{0.3137}$	0.675
Anthesis	Exponential function	$y = 4.9171e^{0.5781x}$	0.646
	Linear function	$y = 2.8686x + 4.9512$	0.645
	Logarithmic function	No result.	
	Polynomial function	$y = 0.41144x^2 + 2.8594x + 4.9402$	0.643
	Power function	No result.	

At anthesis, LCC had the closet exponential relation with the combination of D (NDVI, GNDVI). The monitoring model of winter wheat LCC at anthesis was established by exponential method ($R^2 = 0.646$).

Evaluation of LCC Monitoring Models

A total of 66 samples, which were observed from the experiments at jointing stage (0309), booting stage (0412) and anthesis (0428) in 2012, respectively were used to test the remote sensing monitoring model of winter wheat LCC mentioned earlier. The 1:1 relation diagrams between predicted LCC of established models and measured LCC were drawn to evaluate accuracy of LCC monitoring models. These three remote sensing monitoring models, which were based on the combinations of N (NDVI, GNDVI), R (NDVI, GNDVI) and D (NDVI, GNDVI), respectively, were compared with corresponding single vegetation index models (Fig. 2).

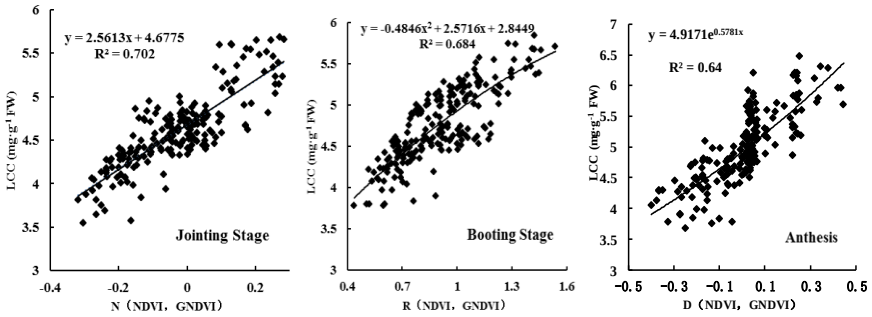

Fig. 1: Remote sensing monitoring model of winter wheat LCC in the key periods

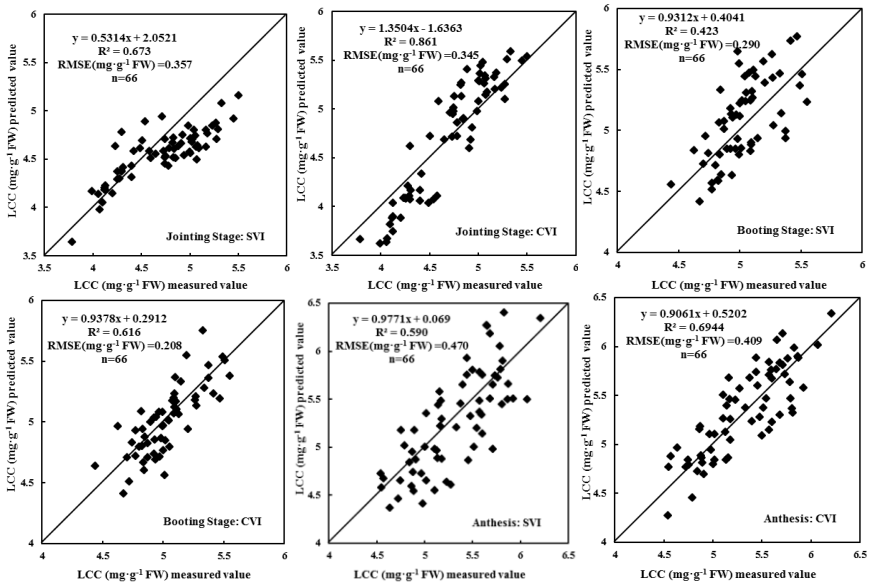

Fig. 2: Reliability testing of the remote sensing monitoring model of winter wheat LCC in the key periods
SVI: Single vegetation index; CVI: Combination of vegetation indices

Employing the vegetation index the most strongly related to LCC as independent variable, the single vegetation index models were established with the modeling method of the simultaneous vegetation index, which was the same with the modeling method of the combination model (e.g., exponential, linear, logarithmic, polynomial and power modeling methods).

The results could be seen from comparison (Fig. 2). At jointing stage, the predicted LCC obtained from the N (NDVI, GNDVI) monitoring model was highly correlated with measured LCC (R^2=0.861, RMSE = 0.345), $R^2$of the N(NDVI, GNDVI) monitoring model was greater than R^2 of the single vegetation index model, and RMSE of the N (NDVI, GNDVI) monitoring model was lower than RMSE of the single vegetation index model, which showed that the N (NDVI, GNDVI) model of monitoring winter wheat LCC was more ideal than the single vegetation index remote sensing monitoring model, and compared to the single vegetation index model, the accuracy of the combination model based on N (NDVI, GNDVI) was improved by 3.4%. Therefore, N (NDVI, GNDVI) was more applicable to remote sensing monitoring of winter wheat LCC at jointing stage. Similarly, because the R (NDVI, GNDVI) monitoring modeling at booting stage showed R^2 = 0.616, RMSE = 0.208 and 15.1% growth of accuracy, it indicated that the R (NDVI, GNDVI) was more applicable to remote sensing monitoring of winter wheat LCC at booting stage. Because the D (NDVI, GNDVI) monitoring modeling showed R^2=0.694, RMSE=0.409 and 13% growth of accuracy, it indicated that the D (NDVI, GNDVI) was more applicable to remote sensing monitoring of winter wheat LCC at anthesis. In conclusion, the combination model based on pair vegetation indices, used to monitor LCC, can improve the monitoring accuracy, so that it is feasible to provide a new method for accurately monitoring crop growth conditions at critical growth stages in the future.

Thematic Maps of Winter Wheat LCC at Critical Growth Stages

Based on the optimal models in Table 4, HJ-1A/1B images in 2014 and the calculation formulas in Table 1,

numerical value maps of sensitive satellite remote sensing variables were generated, which were correctly and effectively calculated one by one. After binaryzation masking, sampling sites were positioned by GPS mentioned earlier and planting area of winter wheat was extracted by supervised classification method. Next, field sampling correction was implemented to promise extraction accuracy of planting area of winter wheat. The remote sensing monitoring diagram of winter wheat LCC spatial distribution during different growth periods in the central region of Jiangsu Province was mapped by using ArcGIS10.3 software to superpose the administrative division vector data of Jiangsu Province covering study areas (Fig. 3).

In Fig. 3, winter wheat LCC in the central region of Jiangsu Province was mainly 4% – 4.5% at jointing stage, 4% –5% at booting stage, and 4.5% –5% at anthesis, which showed a rising trend from the jointing stage - booting stage - anthesis. This result confirmed to the process of winter wheat growth and development of material accumulation process. With the advance of winter wheat to grain maturation, the LCC decreased greatly at later growth stage, and leaf chlorophyll conversion was realized. At the same time, when LCC was completely transformed at the late growth stage, it provided a certain reference for mature harvest. Although the study area was in the central region of Jiangsu Province, the winter wheat LCC in the northern region of Jiangsu Province was higher than that in the central region of Jiangsu Province, which indicated that the growth of winter wheat in the northern region of Jiangsu Province was better than that in the central region.

Discussion

Some researchers prefer to monitor crop growth by multiple parameters or composite indicators (Watts *et al*., 2009; Pagola *et al*., 2012; Tan *et al*., 2015). Most of them focus on single period and could not reflect dynamic changes of crop growth parameters. In this paper, winter wheat LCC at jointing stage, booting stage and anthesis is analyzed to perform dynamic monitoring winter wheat LCC with remote sensing images. We have already found sensitive remote sensing variables of monitoring winter wheat LCC at key growth stages (Fig. 1), which is one of highlights of this paper. The jointing stage sees the most vigorous growth of winter wheat. Nutrient and water management at jointing stage can increase percentage of ear bearing (fertile) and spike number per unit area, thus laying a good foundation for increasing per unit area yield. The booting stage is the key period that determines spike number per mu and number of grain per spike of winter wheat. Enhancing nutrient, water and pest management at booting stage plays an important role in increasing the weight of winter wheat spikes, preventing premature senility in late winter wheat growth period and improving winter wheat quality and output.

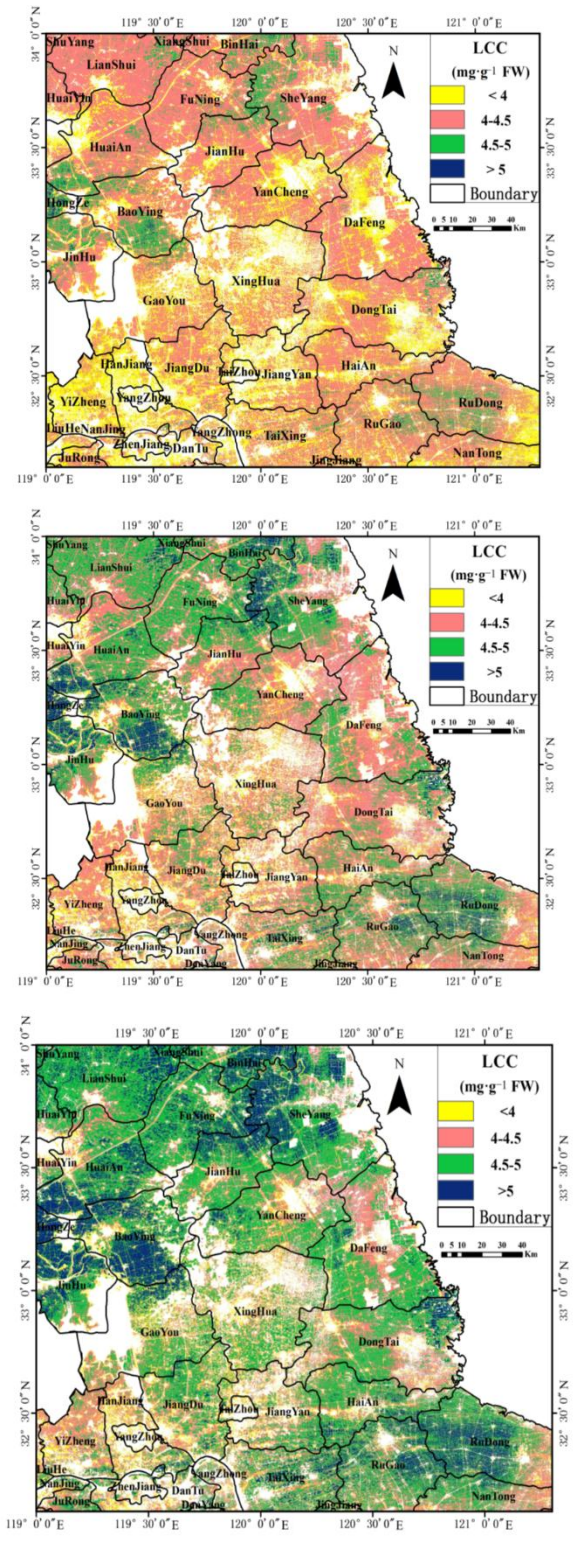

Fig. 3: Mappingwinter wheat LCC spatial distribution in the central region of Jiangsu Province in different periods(Up: Jointing stage; Middle: Booting stage; Below: Anthesis) (The figures were made by employing ENVI5.1 and ArcGIS10.3 softwares)

The anthesis, which is the key stage of winter wheat output and the high-incidence season of pest damages and meteorological disasters, sees the most vigorous metabolism and growth of winter wheat, and scientific and reasonable nutrient and water control at anthesis has important significance to prevent floret degradation, increase setting percentage and increase grains per spike. The authors will connect different growth periods of winter wheat according to LCC increase or reduction range between two adjacent periods, aiming to realize dynamic monitoring of winter wheat LCC and explore the mechanism of substance accumulation.

At present, the hyper spectral remote sensing technique is employed to monitor the LCC, and the spectral information of the target object is obtained at the time of data acquisition. However, the spectral information is the mixed spectrum of all the objects in the receiving range of the probe, and the phenomenon of "homologous isomorphism" and "foreign matter homology" is easy to appear. The canopy image monitoring of crop LCC, based on coverage, to the late growth of winter wheat, because of complete closure line, can only reflect the canopy information, it is difficult to obtain good effect. Tan *et al*. (2012) investigated the fluorescence parameters with the combinations of remote sensing vegetation indices extracted from hyper spectral data, and achieved good results. From this study, it is also found that the LCC of the three critical periods has the strongest correlation with GNDVI, indicating that the GNDVI will tend to be saturated and the vegetation LCC can't be estimated well. In the present study, eight common remote sensing vegetation indices were chosen, namely NDVI, NRI, GNDVI, SIPI, PSRI, DVI, RVI and EVI. They were combined in pairs by difference calculation, ratio calculation and normalization calculation. Therefore, a total of 28×3=84 combinations were gained to promise diversity and reliability. Based on the principle of the strongest correlation and above analysis results, N (NDVI，GNDVI), R (NDVI，GNDVI) and D (NDVI，GNDVI) were chosen to monitor LCC at jointing stage, booting stage and anthesis, respectively. The monitoring model of winter wheat LCC at jointing stage was established by linear method (R^2=0.702). The monitoring models of winter wheat LCC at booting stage was established by polynomial method (R^2 = 0.684). The monitoring model of winter wheat LCC at anthesis was established by exponential method (R^2 = 0.646). The remote sensing vegetation indices combination and the fusion of multiple remote sensing spectral variables can reduce the probability of over-reliance on a certain variable, which is obviously better than the single-band spectral or individual vegetation index.

Previous reports about remote sensing monitoring of crop growth were mostly focused on the quantitative analysis of remote sensing variables and agronomic indicators (Horler *et al*., 1983; Curran *et al*., 1990; Clevers and Gitelson, 2013; Tan *et al*., 2015; Amar *et al*., 2016), existing monitoring models involved easily over-reliance on a particular remote sensing variable, and failed to cover the more remote sensing variables. In this paper, pair remote sensing vegetation indices were combined to make more remote sensing variables to take part in the quantitative analysis, and the massive remote sensing data was limited to a certain extent, which reduced the statistical workload. In order to improve the accuracy of the model, the mechanism and repeatability of remote sensing monitoring were further enhanced. The present study assigned geographic information to map winter wheat LCC at key growth stages, and the quantitative spatial distribution and each grade proportion of winter wheat LCC were intuitively shown by GIS (Geographic Information System) (Fig. 3), so as to indirectly reflect the growth status of winter wheat, provide reliable growth information for crop cultivation management and develop a series of measures to ensure the normal or healthy growth of crop.

This study is based on HJ-1A/1B images. However, extreme weathers easily cause difficulties in surface feature recognition and failure of accurate synchronous sampling, which will influence accuracy of monitoring LCC models directly on large scales. The spectral reflectance extracted from satellite images is crop canopy spectra and the mixed spectrum, and the spatial resolution of the images is much lower than that of the GPS positioning point, which leads to the synchronization between the image and the sampling points. In the future, further studies will be carried out to realize accurate and synchronous monitoring of crop growth with remote sensing. In addition, the authors will explore the physiological cause of winter wheat spectra changes with the growth periods, convert supervision classification to decision tree classification based on multi temporal vegetation index, study how to eliminate the interference, and optimize the extraction method to realize the accurate extraction of winter wheat planting area. Moreover, Future research should expand the sampling to realize satellite – machine (unmanned aerial vehicle, UAV) – ground (in-situ spectra) integration, further optimize remote sensing monitoring algorithm, synthetically consider the complexity of crops and assimilate remote sensing data into the crop growth model with agricultural meteorological data, soil data, cultivation factors and crop varieties information in case of replacing satellite image "area" data with "spot" data, and integrate multi-temporal, multi-dimensional and multi-source remote sensing data so as to enhance the applicability and reliability of remote sensing monitoring.

Conclusion

All in all, the models based on the remote sensing vegetation indices combination can not only increase accuracy of monitoring winter wheat LCC at key growth

stages, such as N (NDVI, GNDVI), R (NDVI, GNDVI) and D (NDVI, GNDVI) were chosen to monitor LCC at jointing stage, booting stage and anthesis, respectively but also provide a new method for accurately monitoring crop growth conditions in the future.

Acknowledgement

Financial assistance for this research was provided by the National Natural Science Foundation of China (41271415, 40801122), a project funded by the Priority Academic Program Development of Jiangsu Higher Education Institutions (PAPD), Fund for Independent Innovation of Agricultural Science and Technology in Jiangsu Province (CX (16)1042), Science and Technology Innovation Group of Yangzhou University, Yangzhou city science and technology project(YZ2016242) and Agricultural Science and Technology Innovation Project of Suzhou City (SNG201643). The Jiangsu map vector data was supported by Yangtze River Delta Science Data Center, National Science & Technology Infrastructure of China. Authors are thankful to the anonymous reviewers and editor for their valuable comments in improving the quality of the manuscript.

References

Al-Abbas, A.H., R. Barr and S.D. Hall, 1974. Spectra of normal and nutrient-deficient maize leaves. *Agron. J*., 37: 3693–3700

Amar, K.D., S. Manisha and M.R. Meshram, 2016. An Analysis of leaf chlorophyll measurement method using chlorophyll meter and image processing technique. *Proc. Comput. Sci*.,85: 286–292

Clevers, J.G.P.W. and A.A. Gitelson, 2013. Remote estimation of crop and grass chlorophyll and nitrogen content using red-edge bands on Sentinel-2 and -3. *Int. J. Appl. Earth Observation Geo inform.*, 23: 344–351

Curran, P.J., J.L. Dungan and H.L. Gholz, 1990. Exploring the relationship between reflectance red edge and chlorophyll content in slash pine. *Tree Physiol.*,7: 33–48

Feng, W., L. He, H.Y. Zhang, B.B. Guo, Y.J. Zhu, C.Y. Wang and T.C. Guo, 2015. Assessment of plant nitrogen status using chlorophyll fluorescence parameters of the upper leaves in winter wheat. *Eur. J Agron*., 64: 78–87

Filella, I. and J. Penuelas, 1994. The red edge position and shape as indicators of plant chlorophyll content, biomass and hydric status. *Int. J. Remote Sens.*, 15: 1459–1470

Gitelson, A.A., Y. Gritz and M.N. Merzlyak, 2003. Relationships between leaf chlorophyll content and spectral reflectance and algorithms for non-destructive chlorophyll assessment in higher plant leaves. *J. Plant Physiol.*, 160: 271–282

Gitelson, A.A., Y. Peng, J.G. Masek, D.C. Rundquista, S. Vermaa, A. Suykera, J.M. Bakerc, J.L. Hatfieldd and T. Meyerse, 2012. Remote estimation of crop gross primary production with Landsat data. *Remote Sens. Environ*., 121: 404–414

Guizar-Sicairos, M., S.T. Thuman and J.R. Fienup, 2008. Efficient subpixel image registration algorithms. *Opt. Lett*., 33: 156–158

Hinzman, L.D. M.E. Bauer and C.S.T. Daughtry, 1986. Effects of nitrogen fertilization on growth and reflectance characteristics of winter wheat. *Remote Sens. Environ*., 19: 47–61

Horler, D.N.H., M. Dockray and J. Barber, 1983. The red edge of plant leaf reflectance. *Int. J. Remote Sens.*, 4: 273–278

Kelly, K.W. and H. Yuhong, 2013. Estimating grassland chlorophyll content using remote sensing data at leaf, canopy, and landscape scales. *Can. J. Remote Sens*., 39: 155–166

Kooistra, L. and J.G.P.W. Clevers, 2016. Estimating potato leaf chlorophyll content using ratio vegetation indices. *Remote Sens. Lett.*, 7: 611–620

Laval-Martin, D.L., 1985. Spectrophotometric method of controlled pheophytinization for the determination of both chlorophylls and pheophytins in plant extracts. *Anal. Biochem*., 149: 121–129

Pagola, M., R. Ortiz, I. Irigoyen, H. Bustince, E. Barrenechea, P. Aparicio-Tejo, C. Lamsfus, S.L. Tang, C. Michel and P. Larouche, 2012. Development of an explicit algorithm for remote sensing estimation of chlorophyll a using symbolic regression. *Opt. Lett.*, 37: 3165–3167

Soummer, R., L. Pueyo, A. Sivarama krishnan and R.J. Vanderbei, 2007. Fast computation of lyot-style coronagraph propagation. *Opt. Express*, 15: 15935–15951

Tan, C.W., X. Yang, M. Luo, C. Ma, X. Yan and T.T. Chen, 2015. Quantitative inversion of key seedling condition parameters in winter wheat at booting stage using remote sensing based on HJ-1A/1Bimages. *Sci. Agric. Sin.*, 48: 2518–2527

Tan, C.W., W.J. Huang, X.L. Jin, J.C. Wang, L. Tong, J.H. Wang and W.S. Guo, 2012. Monitoring the chlorophyll fluorescence parameter Fv/Fm in compact corn based on different hyperspectral vegetation indices. *Spectroscopy Spectral Anal*., 32: 1287–1291

Watts, J.D., R.L. Lawrence, P.R. Miller and C. Montagne, 2009. Monitoring of cropland practices for carbon sequestration purposes in north central Montana by Landsat remote sensing. *Remote Sens. Envir*., 113: 1843–1852

Wessman, C.A., J.D. Aber, D.L. Peterson and J.M. Melillo, 1988. Foliar analysis using near infrared reflectance spectroscopy. *Can. J. Remote Sens.*, 18: 6–11

Yao, F.Q., Z.H. Zhang, R.Y. Yang, J.W. Sun, H.J. Wang and S.G. Ren, 2010. Application of ANFIS in in-situ measured hyperspectral data for vegetation chlorophyll content estimation. *Spectroscopy Spectral Anal.*, 30: 1834–1838

Yoder, B.J. and R.E. Pettigrew-Crosby, 1995. Predicting nitrogen and chlorophyll content and concentrations from reflectance spectra (400-2500 nm) at leaf and canopy scales. *Remote Sens. Environ*., 53: 199–211

Yoshio, I., G. Martine, B. Frédéric, S. Andrew, G. Anatoly, S. Martin, D. Roshanak and O. Albert, 2016. Simple and robust methods for remote sensing of canopy chlorophyll content: a comparative analysis of hyperspectral data for different types of vegetation. *Plant Cell Environ.*, 39: 2609–2623

(Received 17 July 2017; Accepted 15 August 2017)